RSC Advances

PAPER

View Article Online
View Journal | View Issue

Cite this: *RSC Adv.*, 2016, **6**, 8297

Modeling and simulation of an ultrasensitive electron tunneling position/force nanosensor

Zheng Fan,†‡[a] Xinyong Tao,[b] Gautham Dharuman,[a] Xiaodong Li[c] and Lixin Dong*[a]

Received 10th November 2015
Accepted 15th December 2015

DOI: 10.1039/c5ra23781e

www.rsc.org/advances

An ultrasensitive position/force nanosensor model was constructed and theoretically characterized. This model is based on a core–shell nanostructure with an inter-segment nanogap embedded, which forms an alignment-free metal–insulator–metal (MIM) junction. The occurrence of the tunneling effect enables the exponential scaling of the change of the displacement or force using tunneling current, which guarantees an ultrasensitive transduction. The simulation indicates that the combination of proper core materials and optimized design of the nanostructure could highly enhance the transduction performance. The simulation results provide instructions for the implementation of such ultrasensitive tunneling nanosensors, which in turn open new ground for tunneling-effect-based sub-nanoscale or even picoscale position/force detection.

Introduction

It has been 31 years since the invention of the scanning tunneling microscope (STM), which has incomparable spatial resolution based on the electron quantum tunneling effect.[1] However, there have been no other significant applications wherein the same principle of STM in implemented in high resolution transducers. An early attempt can be traced back to the first prototype of the atomic force microscope (AFM), in which an STM was used as the deflection detector, but it was soon replaced with the routinely used laser-lever system due to its large measurement range and readiness for fabrication and alignment. Herein, we report an alignment-free, nanogap-embedded nanowire tunneling picoscope model. Compared with conventional piezoresistive/piezoelectric-effect-based nanoscale position/force transducing,[2–7] sensing based on the tunneling effect could serve the purpose for sub-nanoscale or even picoscale detection due to its exponential dependence on barrier height and width. The proposed model has the potential to serve as an essential foundation for transducers such as pico-newton force sensors, atto-gram mass flow sensors, and single molecule detectors.

[a]*Department of Electrical and Computer Engineering, Michigan State University, East Lansing, MI 48824, USA. E-mail: ldong@egr.msu.edu; Fax: +1 517 353 1980; Tel: +1 517 353 3918*

[b]*College of Chemical Engineering and Materials Science, Zhejiang University of Technology, Hangzhou, Zhejiang 310014, China*

[c]*Department of Mechanical and Aerospace Engineering, University of Virginia, Charlottesville, Virginia 22904-4746, USA*

† Present address: Department of Materials Science and Engineering, University of California, Los Angeles, CA 90095, USA.

‡ Present address: California NanoSystems Institute (CNSI), University of California, Los Angeles, CA 90095, USA.

Modeling

The model is composed of two parts – a mechanical model to determine the relation between the displacement/force and the separation and a tunneling model to obtain the current for the corresponding change in separation. The models are then combined to determine the relation between the displacement/force and the tunneling current. The proposed structure and separation change with the application of force are schematically demonstrated (Fig. 1(a)) and an expanded view of the separation is also illustrated (Fig. 1(b)).

As shown in the schematic of the device (Fig. 1(a)), two conductive nanowires are placed in a row and wrapped concentrically by an insulating nanotube. The area between these two nanowires is a vacuum and the distance is limited to the sub-nanometer range, thus forming a self-aligned nano-constriction.[8,9] A dc bias can be applied to the two ends of both the nanowires, and electrical properties can be measured simultaneously. As the uniaxial loads are applied to the compound concentric nanocylinder from the two ends, the column will remain in equilibrium when the load is smaller than the critical load, F_{cr},[10] and the elastic deformation along the nanowire will cause a decrease in the inter-nanorod separation due to compression. Furthermore, under a force stronger than or equal to the critical load, the column will ultimately buckle and the inner conductive nanorods are deflected accordingly. This is shown in the red box of Fig. 1(a) and a detailed schematic is shown in Fig. 1(b), because the cross-section of the embedded nanorods will rotate accordingly when the nanowire is bent or released. The distance between two corners is then shrunk or expended *via* the change of external force/strain. The buckle modeling of the proposed architecture is performed using the Timoshenko model.

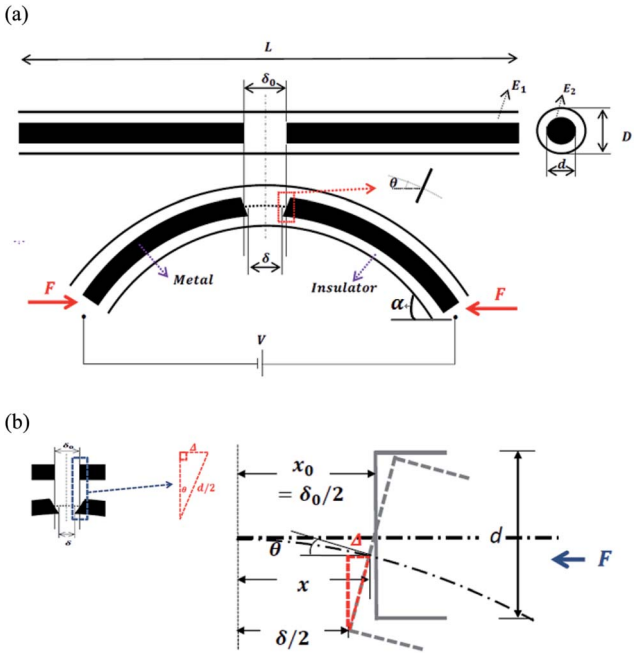

Fig. 1 Schematic of the internal tunneling nanostructure. (a) Proposed structure and the decrease in separation as the nanowire is subjected to external buckling force. E_1 and E_2 are the Young's modulus of the insulating and metallic regions, respectively; δ_0 is the initial separation between the metallic regions; δ is the separation between the lower edges, θ is the angle of rotation of the plane of the metallic region and α is the terminal deflection angle under the action of force; D and d are the outer and inner diameters of the core–shell structure. (b) An expanded schematic for the geometric analysis to obtain relation between separation and angle of rotation.

In the model, the critical force F_{cr}, which is also known as the Euler force, is defined as the axial force that is sufficient to keep the column slightly bent. This can be expressed as[11]

$$F_{cr} = \left(\frac{\pi}{l}\right)^2 (EI)_c, \tag{1}$$

where

$$(EI)_c = E_1 I_1 + E_2 I_2 = \frac{\pi E_1 (D^4 - d^4)}{64} + \frac{\pi E_2 d^4}{64}, \tag{2}$$

l is the chord length of the buckled beam, E_1/E_2 is the Young's modulus of the external/internal nanowire, and D/d is the diameters of the external/inner nanowire. ds represents the differential length of the beam (Fig. 1(a)), then the expression of the length of the deformed beam can be given by[12]

$$l = \int_0^l \mathrm{d}s = \int_0^\alpha \sqrt{\frac{(EI)_c}{2F}} \frac{d\theta}{\sqrt{\cos\theta - \cos\alpha}}, \tag{3}$$

where θ is the angle at the differential segment ds, α is the angle at the terminal of the beam, and F is the magnitude of the buckling force. If we define $k^* = \sqrt{\frac{F}{(EI)_c}}$ and

$$K(p) = \int_0^{\frac{\pi}{2}} \frac{\mathrm{d}\Phi}{\sqrt{1 - p^2 \sin^2 \Phi}} p = \sin\frac{\alpha}{2}, \quad \Phi = \sin^{-1}\left(\frac{\sin\frac{\theta}{2}}{p}\right), \quad \text{and}$$

α defines θ changing from $0 \rightarrow \alpha$, which symbolizes the variation of the terminal angle α, then eqn (3) can be reduced to

$$l = \frac{K(p)}{k^*}. \tag{4}$$

In order to determine the curve of the deformed beam, the coordinates of a differential segment on the deformed axis are given by

$$\mathrm{d}x_i = \mathrm{d}s \cos\theta \tag{5}$$

and

$$\mathrm{d}y_i = \mathrm{d}s \sin\theta. \tag{6}$$

Therefore,

$$x_i = \int_0^\theta \mathrm{d}s \cos\theta = \int_0^\theta \frac{\cos\theta \mathrm{d}\theta}{\sqrt{2}k^*\sqrt{\cos\theta - \cos\alpha}} = \frac{1}{k^*}\left[\int_0^\Phi \left(2\sqrt{1 - p^2\sin^2\Phi}\right)\mathrm{d}\Phi - \int_0^\Phi \frac{\mathrm{d}\Phi}{\sqrt{1 - p^2\sin^2\Phi}}\right]. \tag{7}$$

Moreover, because the incomplete elliptic integral of the first type is given by

$$F(\Phi, p) = \int_0^\Phi \frac{\mathrm{d}\Phi}{\sqrt{1 - p^2\sin^2\Phi}},$$

and the incomplete elliptic integral of second type is[13]

$$E(\Phi, p) = \int_0^\Phi \sqrt{1 - p^2\sin^2\Phi}\, \mathrm{d}\Phi,$$

then eqn (7) becomes

$$x_i = \frac{l}{K(p)}[2E(\Phi, p) - F(\Phi, p)], \tag{8}$$

and in the same way,

$$y_i = \frac{l}{K(p)}[2p(1 - \cos\Phi)]. \tag{9}$$

Herein, since the parameters p, Φ, $K(p)$, $E(\Phi,p)$ and $F(\Phi,p)$ are all correlated to the terminal buckling angle α, the buckling curves (which are symbolized by a series of coordinated points x_i and y_i) can be plotted according to different values of α. The normalized deformed axes $\left(\frac{x_i}{l}, \frac{y_i}{l}\right)$ correspond to the terminal angles of $\alpha = 20°$, $40°$, and $60°$ (Fig. 2(a)).

The buckling of the nanowire induces the deflection of the embedded rods, which in turn modulates the inter-nanorod separation and forms a variable tunneling barrier. The spacing, δ, (Fig. 1(b)) is given by

$$\delta = 2x_i - d\sin\theta, \tag{10}$$

where x_i is the coordinate of the point of interest on the deformed axis corresponding to the terminal angle, α_i, and

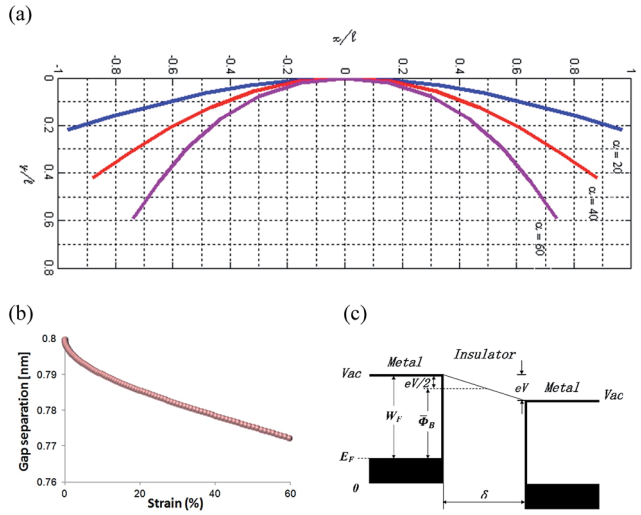

Fig. 2 (a) Normalized deformed axes of the nanowire corresponding to terminal angles of $\alpha = 20°$, 40°, and 60°. (b) Strain-gap separation characterization obtained from the nanowire with the different initial width of 0.8 nm. (c) Potential profile of the metal–insulator–metal junction under the application of a low bias, V. $\bar{\Phi}_B$ is the average barrier height. E_F and W_F are the Fermi energy and the work function of the conductive material, respectively.

$$\sin\theta = 2\sin\left(\frac{\theta}{2}\right)\cos\left(\frac{\theta}{2}\right), \tag{11}$$

where

$$\sin\left(\frac{\theta}{2}\right) = p\,\sin\Phi \tag{12}$$

and

$$\sin\Phi = \mathrm{sn}(u), \tag{13}$$

where $\mathrm{sn}(u)$ is a Jacobi elliptic function, and $u = K(p)\left(\frac{x_0}{l}\right)$.

Herein, the nominal strain, ε, is defined as $\Delta l/l$, which is given by

$$\varepsilon = \frac{\Delta l}{l} = 2\times\left[1 - \frac{E(\Phi,p)}{F(\Phi,p)}\right]. \tag{14}$$

As we substitute eqn (8) and (11–14) into (10), the relation between the separation, δ, and strain, ε, is found as

$$\delta = \frac{l\,F(\Phi,p)}{K(p)}(1-\varepsilon) - 2\,dp\,\mathrm{sn}\left[K(p)\,\left(\frac{x_0}{l}\right)\right]\sqrt{1-p^2\,\mathrm{sn}^2\left[K(p)\,\left(\frac{x_0}{l}\right)\right]}. \tag{15}$$

The strain-gap separation characterizations are obtained from nanowires with the initial width of $\delta_0 = 0.8$ nm (Fig. 2(b)). The curve illustrates a separation decrease tendency corresponding to the increase of strain, which confirms that the gap width can be modulated by simple buckling. Since the gap geometry caused by a specific strain is distinguishable, in principle, each gap is electrically unique at different strain status. This provides the potential to use the unique electrical performance to indicate the dynamics of the displacement.

Moreover, from expression (4) and (10), we can also obtain the relation between the separation and force:

$$\delta = 2x_0 - d\left(\frac{16}{\pi}\sqrt{\frac{F}{EI}}l - 8\right)\sin\left(\sqrt{\frac{F}{EI}}x_0\right). \tag{16}$$

Since the gap distance between each of the two nanorods is within the sub-nanometer range, and the nanowire schematic forms a unique metal–insulator–metal (MIM) architecture, the electron tunneling effect could be addressed.[8,9,14] As we apply the MIM tunneling model here, the approximate expression of the tunneling current density is given by

$$J = \frac{e}{2\pi\bar{h}\delta^2}\left[\bar{\Phi}_B e^{-\frac{\sqrt{8m}}{\bar{h}}\delta\sqrt{\bar{\Phi}_B}} - (\bar{\Phi}_B + eV)e^{-\frac{\sqrt{8m}}{\bar{h}}\delta\sqrt{\bar{\Phi}_B+eV}}\right], \tag{17}$$

where m is the mass of the electron, $\bar{h}$ is the Plank constant, V is the voltage applied between the two electrodes, and $\bar{\Phi}_B$ is the average barrier height between the two electrodes. Then, the potential profile of an MIM junction under a low bias is demonstrated (Fig. 2(c)). The average barrier height is given by $\bar{\Phi}_B = W_F - \frac{eV}{2}$, where W_F is the work function of the inner conductive material. Substituting eqn (15) or (16) into (17) gives the tunneling current *vs.* displacement/force relation.

Result and discussion

Our simulation results have demonstrated the initiation of the tunneling current by the proposed concentric nanostructure. The influence of the external/inner-wire diameter (D/d), initial gap separation (δ_0), nanowire length (L), and material work function (W_F) on the tunneling current under different displacement situations is demonstrated (Fig. 3(a)–(d)). The simulation results indicate the exponential correspondence of the tunneling current to the geometric or electrical properties changes, which indicates the potential of using the proposed nanostructure as a displacement nanosensor.

The force–current curve is also numerically obtained (Fig. 4). It is evident that the maximum current change occurs during the initial stages of buckling, which results in an enormous sensitivity $\left(\frac{\Delta I}{\Delta F}\right)$ of about 6.5 nA nN^{-1} (Fig. 4, inset (ii)) and implies a current increase of 65 pA for every 10 pN increase in force value. This reflects a higher resolution in force sensing as compared to that which works only for a transverse bending force.[15] For the inter-segment structure, in addition to axial force, separation change can also be effected by a transverse force. Versatility in sensing is therefore implicit. Although the sensitivity for this structure is found to have a non-linear curve, a specific region can be selected from the force range depending on the application, and the corresponding sensitivity variation could be linearized. The closed form expression (15) also provides an explanation for the non-zero initial force and the

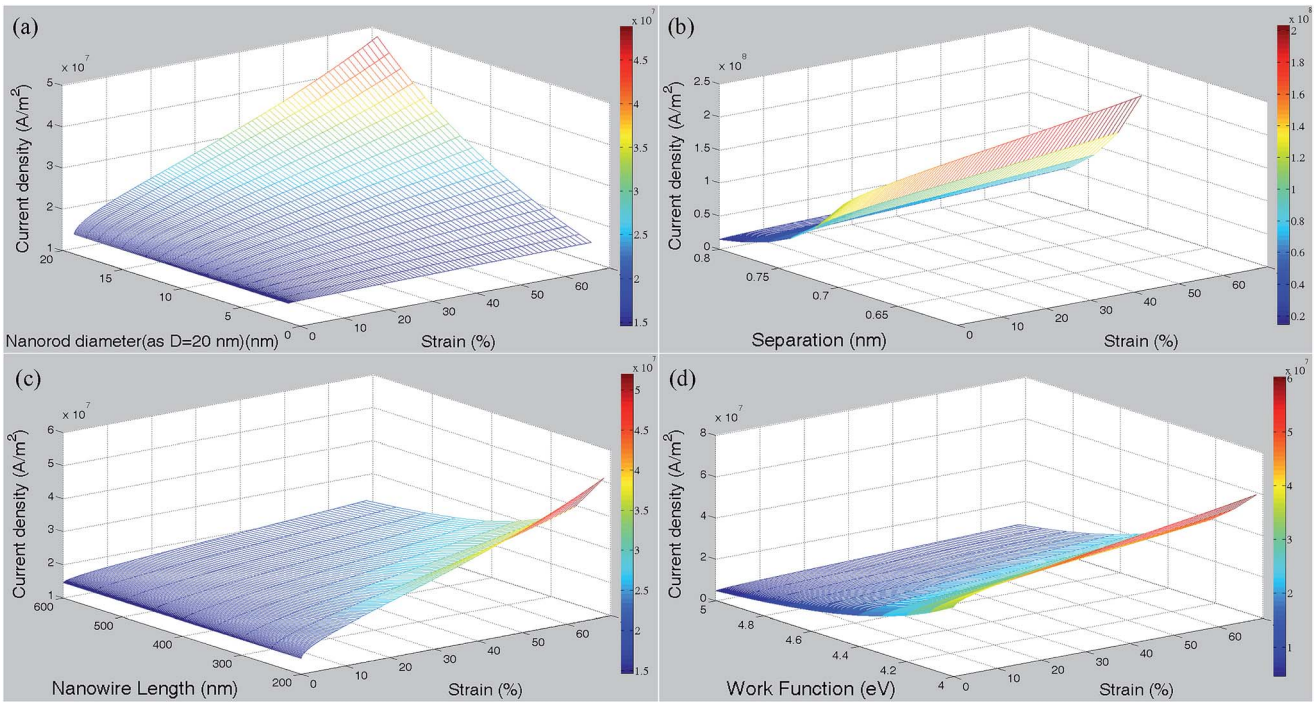

Fig. 3 Simulation results (a) influence of nanorod diameter, d, on tunneling current density. $D = 50$ m and d ranges from 1 to 40 nm. (b) Influence of initial separation, δ_0, on tunneling current density. δ_0 ranges from 0.7 to 0.8 nm. (c) Influence of nanowire length, l, on tunneling current density. l ranges from 200 to 1200 nm. (d) Influence of work function, W_F, on tunneling current density. W_F ranges from 4 to 5 eV.

extent of the decrease in separation. The initial force is non-zero because δ equals the initial value δ_0 when

$$F = \frac{\pi^2 EI}{4l^2} = F_{cr} \quad (18)$$

which is referred to as the critical force,[16–18] *i.e.* the minimum force required to induce buckling and hence cause a change in separation. Since the current enhancement needs to be pronounced, a greater reduction in separation is required. For the same nanowire, this can be achieved by reducing the length while keeping all the other parameters fixed. The effect of reducing the length to one-fourth of its original value is shown in Fig. 5. The reduction in separation is from 1 to 0.92 nm as compared to the reduction from 1 to 0.98 nm for the initial case (Fig. 4, insert (i)). This can also be easily understood from (16) – a smaller length implies greater critical force hence much larger force values are required to cause the same deflection thereby resulting in a much greater reduction in the separation.

Simulations were also carried out for different inner and outer diameters in order to understand their effect on force sensitivity. The current density–force plot for a fixed outer diameter ($D = 20$ nm) and different inner diameters ($d = 7$, 7.5 and 8 nm) are shown in Fig. 6(a). An interesting crossover region is also evident (Fig. 6(a), inset (i)). Also shown is the corresponding separation–force plot (Fig. 6(a), inset (ii)). The

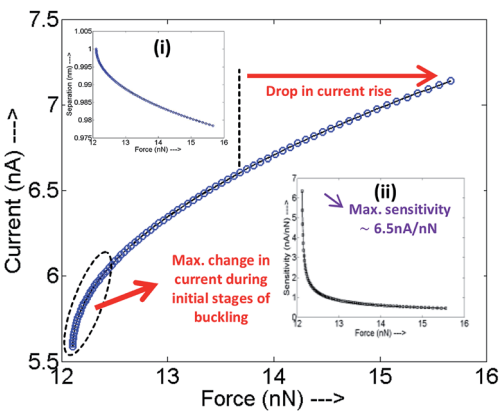

Fig. 4 Current *vs.* force. Insert, (i) current *vs.* force (ii) sensitivity *vs.* force.

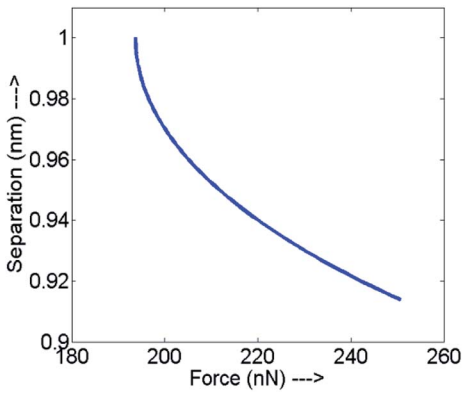

Fig. 5 Greater reduction in separation with a simultaneous shift in the critical force and increased force range compared to the result in Fig. 4, inset (i).

cross over region is a result of the combined flexural rigidity, as in expression (2).

Below the crossover point, the increase in current density is found to be greater for the structure with a smaller inner diameter (Fig. 6, inset (i)), which seems surprising since the opposite effect is expected based on expression (1). However, this can be understood in terms of the critical force in expression (18), which is smaller for a smaller inner diameter (due to the reduced combined flexural rigidity). Beyond the crossover point, the bigger inner diameter structure causes a greater increase in current, which is understood from expression (1). The effect of varying both inner and outer diameters is revealed in the surface plot shown in Fig. 6(b). From this figure, it is evident that the structure with smaller inner and outer diameters has the maximum sensitivity. This can be understood from the previous discussions. Analysis of the current–force and the sensitivity relations for a small difference in inner diameter dimensions is significant when an array of these structures is used for collective sensing. As shown, a difference of even 0.5 nm has a tremendous effect on sensitivity and could therefore result in measurement errors, which can be understood from this model.

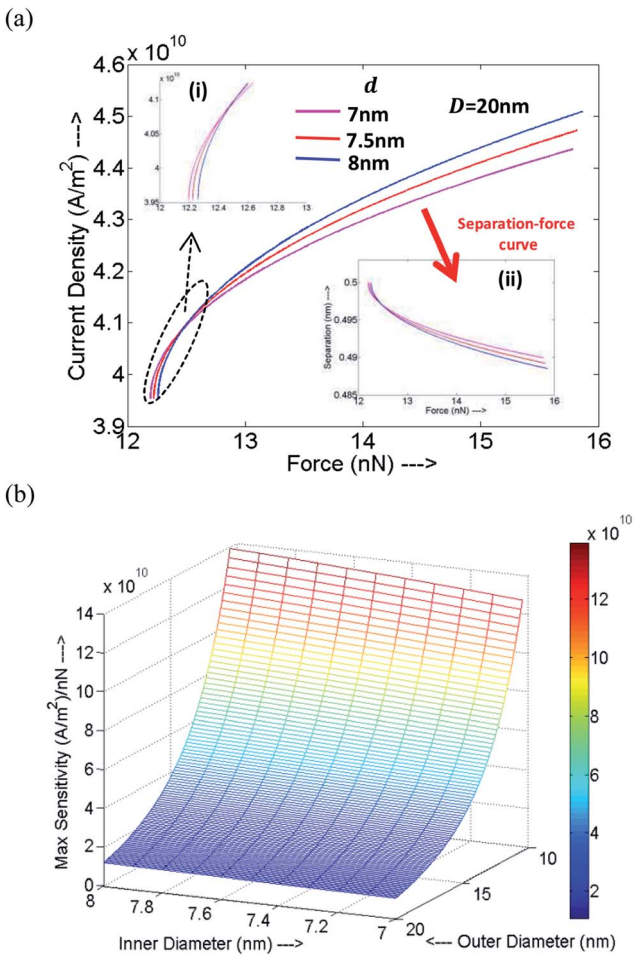

Fig. 6 (a) Current density–force variation for a fixed outer diameter, *D*, and different inner diameters, *d*, insert (i) expanded crossover region, (ii) corresponding separation–force variation. (b) Surface plot showing variation of maximum sensitivity for different inner and outer diameters for the shell–core structure.

Future work

The simulation results indicate the exponential correspondence of the tunneling current to the geometric or electrical property changes of the concentric nanowire. Among them, the change in the initial gap separation and work function of the core materials show a remarkable influence on the tunneling. This information is important for the implementation of the nanowire-based ultrasensitive displacement/force sensor.

In future studies, we plan to synthesize a type of peapod nanostructure based on a boron carbide (B_4C) nanowire,[19] which is encapsulated with a conductive nickel compound nanorod. The distance between each nanorod could be restricted to be smaller than 1 nm, which forms an alignment-free tunneling junction. By applying the TEM nano-manipulator,[20–36] we can select a single nanowire for the *in situ* characterization of its electromechanical properties. Then, the tunneling performance in such proposed inter-segment nanostructure could be studied both theoretically and practically.

Conclusions

In summary, we carried out the modeling and simulation of an ultrasensitive displacement/force nano-transducer based on a nanogap-involved concentric nanostructure. The simulation results indicate that the tunneling performance could be tuned *via* geometric or electrical property changes in the nanowire, especially the core materials and initial gas distance. As a result, by using a combination of carefully chosen core materials and optimized design of the nanostructure, the tunneling performance could be highly enhanced, which in turn improves the sensitivity of such nanowire-based tunneling sensors. The theoretical study provides instructions for the implementation of such nanowire-based sensors. Based on the proposed nanowire architecture as well as the characterization techniques, a nanowire-based inter-segment displace/force nanosensor will be soon realized.

Acknowledgements

This study is supported by the NSF (IIS-1054585), the NSFC (51002138), the Zhejiang Provincial NSF of China (Y4090420), the NSF (CMMI-0968843, CMMI-0824728, CMMI-0653651), the Qianjiang Talent Project (2010R10029), the 'Qianjiang Scholars' program and the project sponsored by the Project sponsored by SRF for ROCS (2010609), SEM.

References

1 D. M. Eigler and E. K. Schweizer, *Nature*, 1990, **344**, 524–526.
2 Y. S. Zhou, R. Hinchet, Y. Yang, G. Ardila, R. Songmuang, F. Zhang, Y. Zhang, W. H. Han, K. Pradel, L. Montes, M. Mouis and Z. L. Wang, *Adv. Mater.*, 2013, **25**, 883–888.

3 J. Zhou, Y. D. Gu, P. Fei, W. J. Mai, Y. F. Gao, R. S. Yang, G. Bao and Z. L. Wang, *Nano Lett.*, 2008, **8**, 3035–3040.
4 R. R. He, X. L. Feng, M. L. Roukes and P. D. Yang, *Nano Lett.*, 2008, **8**, 1756–1761.
5 C. Stampfer, A. Jungen, R. Linderman, D. Obergfell, S. Roth and C. Hierold, *Nano Lett.*, 2006, **6**, 1449–1453.
6 P. Neuzil, C. C. Wong and J. Reboud, *Nano Lett.*, 2010, **10**, 1248–1252.
7 R. R. He and P. D. Yang, *Nat. Nanotechnol.*, 2006, **1**, 42–46.
8 S. E. Kubatkin, A. V. Danilov, A. L. Bogdanov, H. Olin and T. Claeson, *Appl. Phys. Lett.*, 1998, **73**, 3604–3606.
9 D. L. Klein, P. L. McEuen, J. E. B. Katari, R. Roth and A. P. Alivisatos, *Appl. Phys. Lett.*, 1996, **68**, 2574–2576.
10 M. Riaz, O. Nur, M. Willander and P. Klason, *Appl. Phys. Lett.*, 2008, **92**, 103118.
11 S. P. Timoshenko and J. M. Gere, *Theory of elastic stability*, Tata McGraw-Hill Education, New York, 2nd edn, 1961.
12 L. D. Landau, E. Lifshitz, J. Sykes, W. Reid and E. H. Dill, *Theory of elasticity: Vol. 5 of course of theoretical physics*, Pergamon, Oxford, 1959, vol. 5.
13 T. F. Lemczyk and M. M. Yovanovich, *Comput. Math. Appl.*, 1988, **16**, 747–757.
14 J. G. Simmons, *J. Appl. Phys.*, 1963, **34**, 1793–1803.
15 Y. S. Zhou, R. Hinchet, Y. Yang, G. Ardila, R. Songmuang, F. Zhang, Y. Zhang, W. Han, K. Pradel, L. Montes, M. Mouis and Z. L. Wang, *Adv. Mater.*, 2013, **25**, 883–888.
16 C.-L. Hsin, W. Mai, Y. Gu, Y. Gao, C.-T. Huang, Y. Liu, L.-J. Chen and Z.-L. Wang, *Adv. Mater.*, 2008, **20**, 3919–3924.
17 C.-L. Hsin, W. Mai, Y. Gu, Y. Gao, C.-T. Huang, Y. Liu, L.-J. Chen and Z.-L. Wang, *Adv. Mater.*, 2008, **20**, 3919–3924.
18 G.-F. Wang and X.-Q. Feng, *Appl. Phys. Lett.*, 2009, **94**, 141913.
19 X. Y. Tao, L. X. Dong, X. N. Wang, W. K. Zhang, B. J. Nelson and X. D. Li, *Adv. Mater.*, 2010, **22**, 2055–2059.
20 L. Dong, X. Tao, Z. Fan, L. Zhang, X. Zhang and B. Nelson, Nanorobotic spot welding, in *Encyclopedia of nanotechnology*, ed. B. Bhushan, Springer, Netherlands, 2012, pp. 1692–1700.
21 Z. Fan, X. Fan, A. Li and L. Dong, *Nanoscale*, 2013, **5**, 12310–12315.
22 Z. Fan, X. Tao, X. Fan, X. Zhang and L. Dong, *Carbon*, 2015, **86**, 280–287.
23 Z. Fan, X. Y. Tao, X. D. Cui, X. D. Fan, X. B. Zhang and L. X. Dong, *Nanoscale*, 2012, **4**, 5673–5679.
24 Z. Fan, X. Tao, X. Fan, X. Li and L. Dong, *IEEE Trans. Robot.*, 2015, **31**, 12–18.
25 T. Fukuda, M. Nakajima, P. Liu and H. ElShimy, *Int. J. Robot. Res.*, 2009, **28**, 537–547.
26 Z. Fan, X. Tao, X. Li and L. Dong, *Proceedings of IEEE/RSJ 2011 International Conference on Intelligent Robots and Systems (IROS2011)*, 2011, pp. 1705–1710.
27 L. X. Dong, X. Y. Tao, Z. Fan, L. Zhang, X. B. Zhang, H. Huang, M. Hamdi and A. Ferreira, Nanorobotic mass transport, in *Nanorobotics: Current approaches and techniques*, ed. C. M. A. A. Ferreira, Springer, 2012.
28 L. X. Dong, X. Y. Tao, Z. Fan, L. Zhang, X. B. Zhang and B. J. Nelson, Nanorobotic spot welding, in *Encyclopedia of nanotechnology*, ed. B. Bharat, Springer, 2012.
29 Z. Fan, X. D. Fan, A. Li and L. Dong, *Proceedings of the 12th IEEE Conference on Nanotechnology (IEEE-NANO 2012)*, 2012.
30 Z. Fan, X. Y. Tao, X. B. Zhang and L. Dong, *Proceedings of the 12th IEEE Conference on Nanotechnology (IEEE-NANO 2012)*, 2012.
31 J. Du, Y. C. Yang, Z. Fan, Y. Xia, X. J. Cheng, Y. P. Gan, H. Hang, L. X. Dong, X. D. Li, W. K. Zhang and X. Y. Tao, *J. Alloys Compd.*, 2013, **560**, 142–146.
32 Z. Fan, M. Yu, X. Y. Tao, R. Shanmugam, X. Fan, W. Lai and L. Dong, *Proceedings of the 14th IEEE Conference on Nanotechnology (IEEE-NANO 2014)*, 2014.
33 G. Dharuman, Z. Fan and L. Dong, *Proceedings of the 13th IEEE Conference on Nanotechnology (IEEE-NANO 2013)*, 2013.
34 X. Y. Tao, J. Du, Y. P. Li, Y. C. Yang, Z. Fan, Y. P. Gan, H. Huang, W. K. Zhang, L. X. Dong and X. D. Li, *Adv. Energy Mater.*, 2011, **1**, 534–539.
35 Z. K. Weng, L. Dong, M. Yu, F. B. Rao, Z. Fan and Z. B. Wang *Proceedings of the 13th IEEE Conference on Nanotechnology (IEEE-NANO 2013)*, 2013.
36 X. Tao, Z. Fan, B. J. Nelson, G. Dharuman, W. Zhang, L. Dong and X. Li, *Nano Lett.*, 2015, **15**, 7281–7287.

